Tomographic Wave Front Sensing using a Single Imaging Shack-Hartmann Wave Front Sensor and Multi-Frame Blind Deconvolution

Matthew Willson
Georgia State University, GA, USA
Stuart M. Jefferies
Georgia State University, GA, USA
University of Hawaii, HI, USA
Douglas A. Hope
Hope Scientific Renaissance L.L.C., CO, USA

August 2018

Abstract

Current methods for correcting imagery that has been acquired through atmospheric turbulence typically rely on the assumption that the turbulence is concentrated in the aperture of the telescope. In this case the atmospheric point spread function (PSF) is spatially invariant across the field of view and the image can be modeled as a convolution of the target object intensity with the PSF. This is a reasonable assumption for small fields-of-view that are commensurate with or less than the isoplanatic angle for the atmosphere. However, for fields-of-view larger than the isoplanatic angle the PSF varies with position in the image. This is because the nature of the atmosphere is in fact three-dimensional and the turbulence sampled by two different field points can be significantly different depending on the height profile of the turbulence. Thus any correction of an image that covers multiple isoplanatic angles, based on a spatially invariant PSF, will suffer degradation. By modeling the atmosphere as a set of independent "frozen" layers, each propagating across the telescope aperture with their local wind velocity, we show it is possible to both separate out the composite layers of the atmosphere, and arrange the layers at appropriate heights to produce PSF estimations which remain robust across multiple isoplanatic angles.

1 Introduction

While in truth the atmospheric turbulence which inhibits high resolution imaging with large aperture telescopes is present over a wide range of altitudes within the atmosphere, the worst of the distorting effects are generated within narrower altitude ranges where the properties of the atmosphere change between different atmospheric layers. This allows for a simplified approach of considering the distortion as a summation of the effects caused by each layer. When correcting for the atmospheric turbulence, the 3-dimensional nature of the turbulence results in limiting the effectiveness of any correction which relies on measuring the composite phase caused by the turbulence to within an isoplantic angle. As conditions can change rapidly over the course of an observation, this can result in a severe degradation of data and a harsh reduction in the resolution of the retrieved image.

Here we detail a method for splitting the phase information in the telescope aperture, as measured using an imaging Shack-Hartmann sensor (ISHS), into a set of independent turbulent layers using the frozen flow hypothesis and knowledge that the layers propagate with unique wind velocities. With the separated layers we then show how to obtain the remaining 3-dimensional information through the use of an off-axis guide star and a grid-based fitting routine to find the heights of each of the layers. Combining the techniques together, we show their effectiveness in retrieving superior phase information within and beyond the isoplanatic angle.

2 Separating the atmospheric layers

Imaging Shack Hartmann sensors have, to date, been primarily employed for wave front sensing in solar adaptive optics systems (4). Here the Shack-Hartmann sensor is configured to provide a critically sampled image of the object through each sub-aperture rather than the under-sampled images typically made by this type of sensor. Traditionally, the retrieval of the wave front phase information from an ISHS is obtained by taking the image formed by one of the micro-lenses and cross-correlating it against the images formed by all the other micro-lenses. The offsets of the peaks of the resulting cross-correlation functions, from the plane-wave reference points, are then used to determine the gradients of the wave front phase. These, in turn, are integrated to provide an estimate of the wave front phase in the pupil.

The main drawback of this type of analysis of ISHS data is that it recovers only the wave front slope in each sub-aperture: it is blind to fine structure within the sub-aperture. However, this limitation can be overcome by using a phase retrieval algorithm to recover the wave front information in each sub-aperture (5; 6). In this case the resolution of the wave front estimate is only limited by the resolution of the pixel array used to record the ISHS image data (5). As stated above, the resolution of the pixel array for recording the image data is normally set such that we achieve Nyquist sampling of the images from the sub-apertures. However, this can be improved on. For short intervals the turbulence in the different atmospheric layers can be considered as frozen and propagating across the telescope aperture with the local wind velocity. This behavior can be leveraged to recover spatial frequency information on the wave front that is finer than that sampled by the recorded images (7). Practically this is accomplished by using a phase retrieval algorithm that accounts for the temporal phase correlations inherent in the observed wave fronts. This is the approach we take in the work reported here.

For phase retrieval we use the multi-frame blind deconvolution (MFBD) technique of Hope et al. (1). Here the wave front phases are modeled using a multi-layer model for the atmosphere where the layers remain frozen and propagate with different velocities (7). The algorithm assumes isoplanatic imaging and all of the atmospheric layers in the model for the data are located in the telescope aperture. This assumption restricts us to imaging a small field-of-view.

As with any MFBD algorithm, it is important to provide the best possible initial estimates for both the object being observed and the atmospheric point spread functions (modeled using estimates of the atmospheric wave front phases). In addition, for the Hope et al. MFBD algorithm (1) we also need to know the number of layers to use in our model for the atmosphere, along with the corresponding wind velocities [ref]. We obtain this information through an analysis of the 3-D autocorrelation function of the gradients of the phase estimates obtained by a tradition treatment of the Shack-Hartmann. For the initial estimates of the wave front phases we use the tip/tilt components of the phases in each sub-aperture as determined from the centers-of-masses of each of the images from the sub-apertures.

We note that although the information needed to recover the wave front amplitude is readily available in the measured intensities of the images from the micro-lenses, we don't use it here. This is because we assume that we are observing at a low-Zenith angle and we can ignore the effects of scintillation. We plan to upgrade our phase retrieval algorithm to accommodate wave front amplitude estimation, in the near future.

We note that the main advantage of our MFBD approach to phase retrieval, over the other phase retrieval algorithms that have been used with ISHS data to date (5; 6), is that we leverage the temporal correlations that are inherent in the atmospheric wave fronts. Basically, including temporal correlations through a frozen flow model increases the spatial resolution of the recovered wave fronts and enables physically meaningful estimates of the phases in the individual atmospheric layers. It also reduces sensitivity to piston errors in the phase estimates at the boundaries of the sub-apertures that are incurred in other approaches (e.g., (5)). A secondary advantage is that we can image any type of target: it does not have to be a point source.

Now, there are two mechanisms that can provide leverage for estimating the wave fronts in the individual atmospheric layers: the geometry of the micro-lens array, and the frozen flow behavior of the layers. This is demonstrated in Figure 1. For the former to be practically useful we need to know the heights of the layers. The latter does not have this restriction. We are therefore able to separate the layers even though they are all assumed to lie in the pupil plane in the MFBD algorithm. The fidelity with which we can do this is shown in Figure 2. Once we have physical estimates for each of the layers we can then use the leverage provided by the micro-lens geometry to determine the heights of the layers. That is, we use the fact that the best match of our image model to the data should occur when we have the estimated layers located at

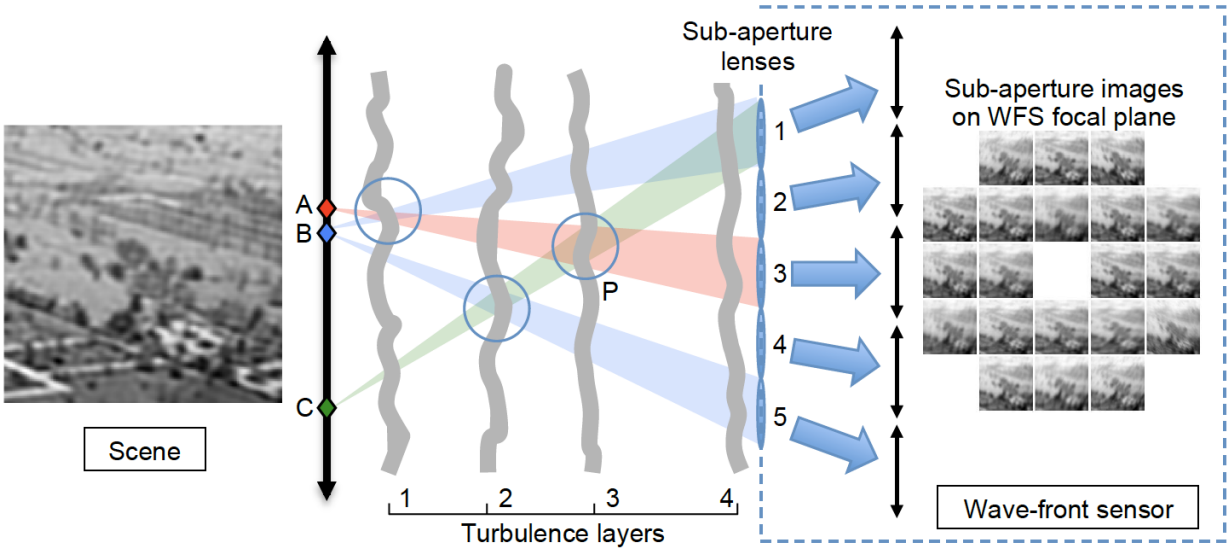

Figure 1: Cartoon of how tomography is enabled using an imaging Shack-Hartmann sensor. I) Geometry: at any given time there are multiple field points that sample the same region of turbulence (for example, region P in layer 3 is sampled by field points A in the image from sub-aperture lens 3 and C in the image from sub-aperture lens 1). II) Frozen flow behavior of atmosphere: there are multiple field points that sample the same region of turbulence at different times (e.g., the turbulence sampled by field point C by sub-aperture lens 1 at time t_0, is sampled by field point B at time $t_0 + \delta t$ by some other sub-aperture that depends on the velocity of the layer). Cartoon is courtesy of Michael Hart.

their correct heights. It is this aspect of the tomography problem that we investigate here.

3 Tomography

To develop the algorithm for solving for the layer heights, we simulated a data set collected from a 3.6 m diameter (D) telescope containing a 0.2 m perforation through a turbulent atmosphere with a characteristic size $r_0 \sim$ 6cm at $0.5\mu m$. This corresponds to a data set with D/r_0 of ~25 at the observing wavelength ($1\mu m$) and represents poor seeing conditions on Mount Haleakala on Maui.

We simulate an atmosphere containing three layers, each possessing identical properties but consisting of independent random draws. These layers are equally weighted and fixed to heights corresponding to pupil (0 km), intermediate (5 km) and upper atmospheric layers (15 km). To simulate recovered phases, as if found through use of the MFBD algorithm, we convolve the 'truth' phases screens with a Gaussian profile such that the RMSE difference between the truth and blurred phases is ~0.25 rad, typical of the recovered phases produced by our MFBD algorithm for $D/r_0 \sim 25$ conditions.

The method for approaching the estimation of the height relies on treating each layer independently and solving for the height separately. Completing a full grid search of the available parameter space at a 1 km resolution for three layers results in 20×20×20 number of models to test. By making the assumption that at least one layer lies in the pupil plane and that the layers can be fitted for independently from one another, this narrows the parameter space down to at most 5×20 models if the order of the heights it unknown. If the order is known, then the parameter space is confined to 20+20 models. Further, if an assumption that the layers come from distinct regions in the atmosphere (i.e top layer is between 10 - ,20 km, middle between 1 - 10 km) then this parameter space can be even further restricted. A schematic for the algorithm is shown in Figure 3.

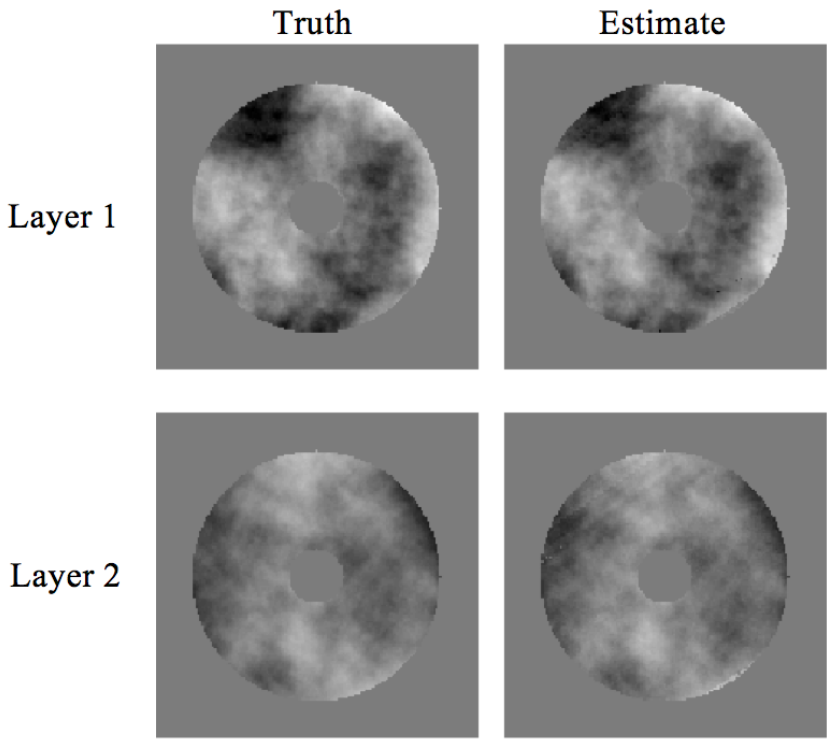

Figure 2: Wave-front phase after removal of global tip/tilt: layer 1 (top row) layer 2 (bottom row). The true phases are in the left column; the estimated phases are in the right column. The images in each row are displayed on the same linear scale. The estimated phases were recovered from ISHS data obtained with a 6x6 micro-lens array using our MFBD algorithm. The object being imaged was a satellite and the level of turbulence in the composite phase is $D/r_0 \sim 25$. The RMSE difference between the truth and blurred composite phases is $\sim$0.55 rad,

Taking in the separated phase screens, all are initially assumed to be in the pupil layer or at a height of 0 km. At this stage, no assumption of order of the layers is made. The height order of the layers is found by performing an unrestricted least squares fit except to require that all heights are positive and no higher than 30 km.

The produced fit is typically poor as an analytical gradient is very difficult to calculate. Instead a numerical gradient had to be computed which results in a typically inaccurate measurement of the heights of the layers which is not useful in increasing the Stehl of PSFs outside of the isoplantic angle. This initial stage is useful however in that it does enable an initial height order to be established through taking the order of the layers based on how much they changed from their initial height, with the fitted heights for phase screens higher in the atmosphere changing more than phase screen representing lower layers.

Taking this order as a starting point, all layers are set to zero again except the phase screen determined to be the top layer. A coarse grid search over a range of heights for the top layer is performed. For each height, an image is computed and compared to the 'real' image as the squared difference between the two images. The smallest difference is then used to determine the best height for the top layer. If there is a range of heights for which equally good fits are achieved then a mean of these heights is used.

An identical process is then performed for subsequent layers moving down through the atmosphere, except with the previous layers fixed to their found heights. The final layer is always fixed to the pupil layer.

For data sets in which knowledge of the phase screens used to generate 'real' images is perfect and contains three layers (layer heights = 0 km, 5 km, 15 km, D/r_0=5-25), this algorithm is robust and recovers the heights in all cases to an accuracy of better than 1 km. In these perfect cases, Strehls of > 0.95 are

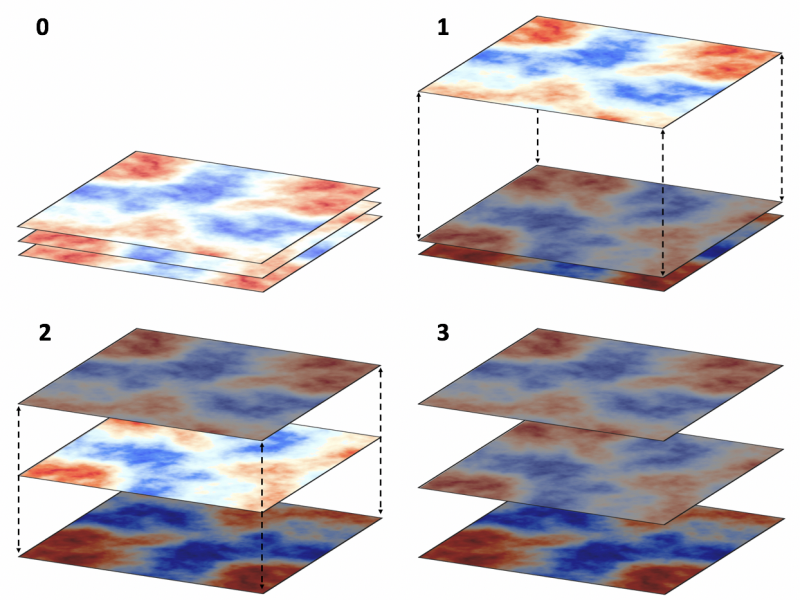

Figure 3: Schematic showing the stages of the height fitting algorithm. Step 0: An initial estimate for the height of each layer is made through a least squares fit in which the height of all the layers in free to change. The gradient in this fit is computed numerically. Step1: Using the height order established in step 0, the lower two layers are set to a height of 0 km (i.e the pupil plane) while a grid fit is performed for the highest layer. Step 2: The height found for the top layer in step 1 is used to fix the top layer height during the grid fit for the middle layer. The bottom layer remains fixed to the pupil plane. Step 3: The best fit results for the heights are returned. If an insufficiently small improvement to the PSF estimation compared to the estimate from step 0, then the order of the heights is rotated and the process starts again from step 1.

readily obtainable. Furthermore, the algorithm remains robust in retrieving the layer heights in the case where an additional phase screen is used to generate the data which is not included in the fits, simulating a hypothetical case in which the MFBD algorithm fails to detect a weaker atmospheric layer.In this scenario, while the heights of the fitted layers are again retrieved to better than 1 km accuracy, due to missing phase information contained in the absent phase screen, the correction suffers but this effect is uniform across the field of view. The degree to which the correction suffers is proportional to the strength of the phases contained in the missing phase screen. In all these cases, only a single off-axis 'guide star' is required.

Next we test the performance of the algorithm when dealing with the simulated recovered phases. The result is a smaller improvement to the mean square difference calculations used in the coarse grid fits, used as a measure of the goodness of fit. To enable fitting with degraded phase screens, a requirement is placed within the algorithm that the improvement to the mean square difference be at least 10% of initial unrestricted least square fits. If after a grid fit has been performed for a layer and the improvement is under this condition, the order of the heights is rotated under the assumption that the initial order found was incorrect. In the case where all possible orders are tried and none are found to exceed this condition, the order in which the best improvement was found is used. This method increases the computational cost of the algorithm, but as there is a maximum of 6 possible orders for a three layer atmosphere which treated in this way (three for the top layer, two for the middle layer), it is not excessive. The accuracy to which the heights are retrieved is not as accurate in this case but still reliably to within 2 km. This enables a strong improvement to PSF estimations outside the isoplantic angle, see Figure 4. In all these cases, the

For a fit accurate to within 1-2 km on a target at an altitude of 400 km and using 'truth' phases (i.e. unblurred, representing perfect knowledge of the atmospheric turbulence in the absence of noise), we find this level of accuracy to be sufficient to produce a perfect correction. Degrading the input phase screens, there remain residuals and artefacts, but these are small and more uniform compared to the isoplanatic

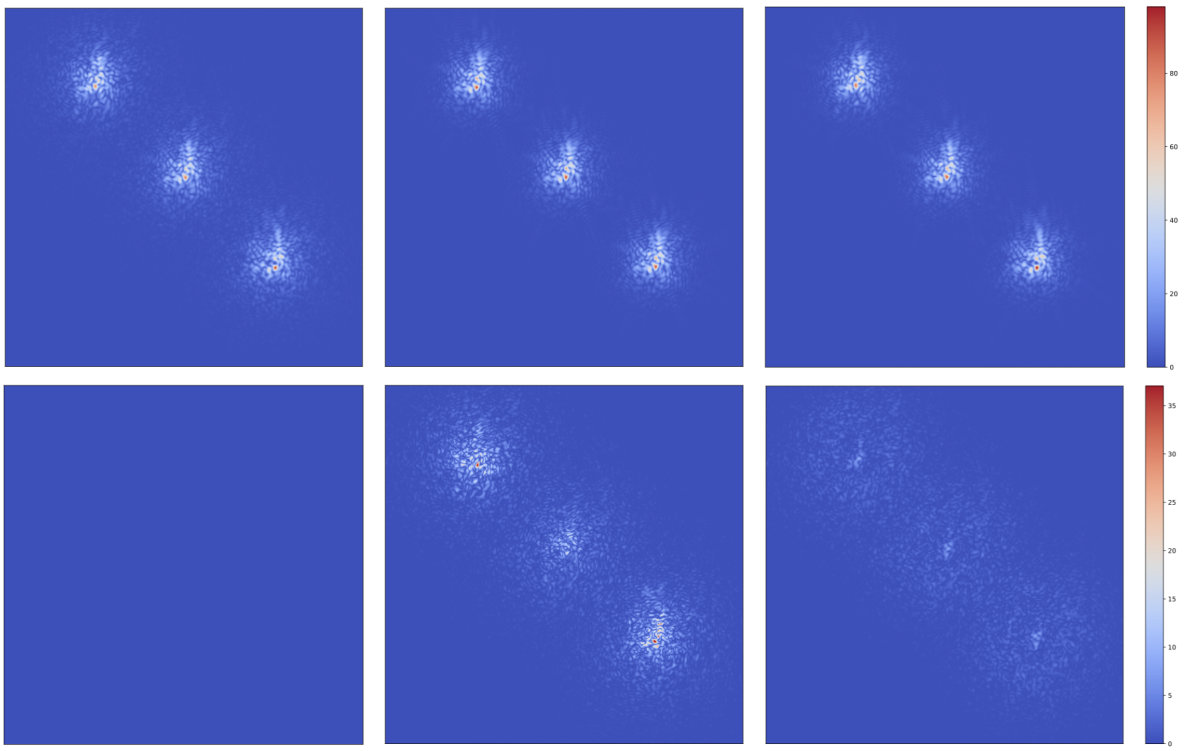

Figure 4: Figure showing PSFs generated using isoplantic and non-isoplantic phases screens representing a simplified and more physical model of atmospheric turbulence. Field of view covers ∼10 isoplantic angles. Top row, left: 'True' images generated using three random draw phase screens. The phases used in the middle and right columns are identical to those used in the first column but have been convolved with a Gaussian profile such that the RMSE between the three screens and the 'true' phases are typical of those found by our MFBD algorithm, see Section 3. We refer to these phase screens as being 'blurred'. This removes much of the higher frequency information and makes finding an accurate height for the layers more challenging. The heights of the layers have been set to 0, 5, and 15 km respectively. Middle column: Treatment of the artificial image as an isoplanatic atmosphere where all phase is assumed to be within the pupil layer, i.e. all layers have a height of 0 km. Bottom column: Treatment of the atmosphere where the heights of the layers is found using the algorithm described in Section 4 (0, 4, and 13.5 km); Bottom row: RMS residuals between the 'True' image in the top left panel and the corresponding image above. Left: Perfect correction. Middle: Decent correction for the central PSF with the exception of the high frequency information loss in the blurred phase screens. This is untrue of the outer PSFs however which show strong residuals after the correction. This is due to them being positioned outside the isoplantatic angle. Right: Correction is more even across the field of view due to the layers being positioned near to their correct heights. Remaining residuals are due to the loss of high frequency information in the blurred phase screens.

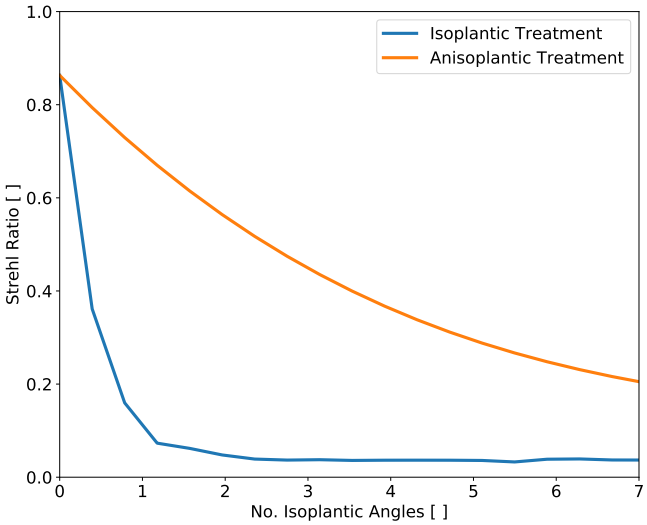

Figure 5: Plot comparing the Strehl as a funciton of radius for isoplanatic and anisoplanatic treatments. The isoplanatic case (blue) shows the strong drop in Strehl as the radius increases to 1 isoplanatic angle. The anisoplanatic case is more robust to the increase in radius, remaining near difraction limited at 1 isoplanatic angle and only falling below a Strehl of 0.1 beyond 7 isoplanatic angles.

treatment.

To test the improvement of the PSF estimations beyond the isoplanatic angle, we compute Strehl's across a range of radii covering 0-7 isoplanatic angles. We subtract the model phases from the truth phases at each position and produce a PSF from the residuals. The peak flux from this residual PSF is compared to the peak flux from the diffraction limited PSF to find the Strehl. The results are shown in Figure 5.

When all layers are assumed to be in the pupil we see the expected drastic drop in the Strehl as we cross the first isoplanatic patch. By a radial distance of one isoplanatic patch, the Strehl has reduced to below 0.1 where it remains for all larger radii.

In the anisoplantic case, the correction remains far more robust to increasing radii, with the Strehl dropping from ~ 0.86 to ~ 0.6 at 1 isoplanatic angle. By 4 isoplanatic angles, the Strehl has dropped to ~ 0.4 displaying the great improvement to the effective field of view when the heights of the layers are accounted for.

4 Conclusion

Through the use of the propagation of the atmospheric layers responsible for distorting the incoming wavefront across an aperture and the assumption of a frozen flow model, we show that it is possible to accurately measure the atmospheric phase at sub-pixel resolutions. Further, we show that it is possible to separate out the individual layers from the composite phases observed in the aperture.

Using the separated atmospheric layers from this method, we show that it possible to solve for the heights of the layers to an accuracy of $\sim$1 km,or better, even in cases where the measured phases are strongly degraded compared to the truth phases. With the heights and separated layers it is then possible to produce accurate PSF estimations beyond the isoplanatic angle, enabling a robust correction which can stretch across multiple isoplanatic angles with a drop in the Strehl of 0.86 to 0.6 over 2 isoplanatic angles. This is a considerable improvement over current treatments which fail rapidly beyond a single isoplanatic angle (Strehl falls to 0.1 over 2 isoplanatic angles).

5 Summary

In this paper we have shown that tomographical wavefront sensing is possible with a single Shack-Hartmann wavefront sensor. We derive the 3-dimensional phase information of the atmosphere in two steps. First we use a MFBD algorithm with the ISHS image data to determine the number of atmospheric layers we need to model the data and to then extract phase estimates for each of these layers. We then use this information to determine the heights of the layers that provide the best match to the observed data. With this information we have shown that it is possible to achieve excellent image correction both within and beyond the isoplanatic angle.

Applying these techniques will enable an observer to not only observe over a wider field of view but also to improve upon current high contrast imaging techniques. Over the course of an observation, the size of the isoplanatic angle can vary be a factor of two or more within within a few tens of milliseconds. The result of this drastic variance of the image is a reduction in the fidelity of the PSF estimation and hence a residual 'cloudy' artifact in the final reconstructed image. These artifacts presently limit the contrast sensitivity obtainable with post processing techniques. By including the altitudes of the atmospheric turbulence layers, one can do a superior job of reducing this effect and hence improve the contrast sensitivity of an observation, even in poor conditions. Furthermore, this enables an observer to move further away from the zenith, increasing the area of the sky observable from a single location. These regions of the sky have smaller values of r_0, and are more susceptible to the kind of strong variance in the strength of turbulence over the course of the night.

Not only do these new techniques allow one to observe more of the sky within a single frame, but also enable access to an observer to a wider portion of the sky at high Strehl ratios.

Bibliography

[1] D. Hope, S. M. Jefferies, M. Hart, and J. Nagy, *High-resolution speckle imaging through strong atmospheric turbulence*, Optics Express, 24, 12116-12129, 2016.

[2] S. M. Jefferies and J. C. Christou, *Restoration of Astronomical Images by Iterative Blind Deconvolution*, Astrophysical Journal, 415, 862-864, 1993.

[3] D. A. Hope and S. M. Jefferies, *Compact multi-frame blind deconvolution*, Optics Letters, 36, 867-869, 2011.

[4] T. Rimmele and J. Marino, *Solar adaptive optics*, Living Reviews in solar physics, 8, 2 2011.

[5] M. Aubailly and M. Vorontsov, *Scintillation resistant wave front sensing based on multi-aperture phase reconstruction technique*, J. Opt. Soc. Am. A., 29, 1707, 2012.

[6] A. Polo, N. van Marrewijk, S.F. Pereira and H.P. Urbach, *Extreme Ultraviolet (EUV) Lithography III*, edited by Patrick P. Naulleau, Obert R. Wood II, Proc. of SPIE Vol. 8322, 832219 2012.

[7] S. M. Jefferies and M. Hart, *Deconvolution from wave front sensing using the frozen flow hypothesis*, Optics Express, 19, 1975-1984, 2011.